Available online at www.sciencedirect.com
ScienceDirect
Journal of Sound and Vibration 319 (2009) 832–849
JOURNAL OF SOUND AND VIBRATION
www.elsevier.com/locate/jsvi

Experimental identification of viscous damping in linear vibration

A. Srikantha Phani, J. Woodhouse*

Department of Engineering, University of Cambridge, Trumpington Street, Cambridge CB2 1PZ, UK

Received 20 April 2007; received in revised form 14 June 2008; accepted 16 June 2008
Handling Editor: C.L. Morfey
Available online 19 August 2008

Abstract

This paper is concerned with the experimental evaluation of the performance of viscous damping identification methods in linear vibration theory. Both existing and some new methods proposed by the present authors [A.S. Phani, J. Woodhouse, Viscous damping identification in linear vibration, *Journal of Sound and Vibration* 303 (3–5) (2007) 475–500] are applied to experimental data measured on two test structures: a coupled three cantilever beam with moderate modal overlap and a free–free beam with low modal overlap. The performance of each method is quantified and compared based on three norms and the best methods are identified. The role of complex modes in damping identification from vibration measurements is critically assessed.

1. Introduction

In a previous paper [1], methods for identifying the parameters of a non-proportional viscous damping model were classified into three groups: matrix methods based on the measured frequency response function (FRF) matrix, modal methods based on fitted modal parameters obtained from FRFs, and enhanced methods which combine the two approaches. The performance of these groups of methods in selected simulation test cases has been presented in Ref. [1]. In the present work the performance of the same set of identifications methods is evaluated on two test structures via experiments. The two test structures will be described in Section 2. Specific sources of errors relevant to the experiments which can potentially influence the outcome of damping identification methods will be discussed in Section 3. The results of damping identification methods are presented for the two test structures in Sections 4 and 5. The major outcomes of the present study are summarised in Section 6.

2. Test structures

The first test structure to be considered comprises three cantilevers coupled at their base. The test structure is shown in Fig. 1. This structure is fabricated by making slots in a mild steel rectangular plate of 2 mm

*Corresponding author. Tel.: +44 1223 765925; fax: +44 1223 332662.
E-mail address: jw12@cam.ac.uk (J. Woodhouse).

0022-460X/$ - see front matter © 2008 Elsevier Ltd. All rights reserved.
doi:10.1016/j.jsv.2008.06.022

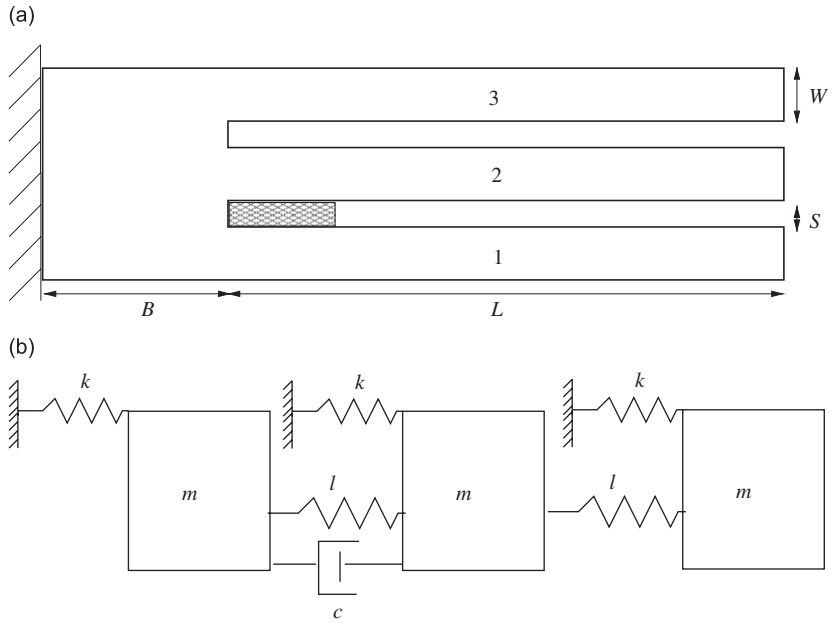

Fig. 1. (a) Experimental set-up for the three cantilever system. The geometric parameters are $B = 150\,\text{mm}$, $L = 400\,\text{mm}$, $S = 10\,\text{mm}$, $W = 20\,\text{mm}$. All beams are prismatic with 2 mm thickness. The main source of damping in this test structure is a wedged foam between beams 1 and 2 (shown here as a shaded patch). (b) A spring–mass–dashpot model for the test structure in each pass band.

thickness. Localised damping is added, in the form of a wedged foam block, indicated by the shaded rectangle in the figure. The choice of this test structure was motivated by the ease with which the modal overlap can be controlled by varying the details of the added damping and the geometry of the structure, such as the dimensions L, B, W and S (see the figure for the definition of these parameters). The modal overlap factor μ_{kn} is defined as $\mu_{kn} \equiv \zeta_n\omega_n/(\omega_k - \omega_n)$, where ω_n and ζ_n denote the natural frequency and modal damping factor of the respective modes indicated in the subscript. It has been shown in an earlier simulation study [1] that modal overlap has a strong influence on the complex modes and hence on damping identification. In this context, the coupled cantilever structure provides an ideal test bench to compare the performance of damping identification methods in a system with moderate overlap. The observed modal overlap factors were in the range 1–2%.

Given the spatially repetitive nature of this structure along its width, it is expected that its frequency response will show characteristic stop and pass bands. Each pass band contains three modes corresponding to the individual flexural modes of the three cantilevers. Thus in the first pass band, each beam vibrates in its first flexural mode while in the second pass band each beam vibrates in its second mode and so on for higher pass bands. Typical mode shapes of the three modes in the third pass band, obtained using a finite element (FE) model of the test structure, created in ABAQUS, are shown in Fig. 2. The FE model allows one to study the influence of the geometric parameters on the modal spacing. This allowed the design of a test structure with desired modal spacing such that each peak can be fitted using standard modal parameter identification methods without much difficulty.

A discrete spring–mass–dashpot model which can be used to represent any single pass band of the test structure is sketched in Fig. 1(b). Here, each cantilever is idealised as a mass and spring corresponding to the modal mass and stiffness, respectively, and the base plate is idealised as a weak spring coupling the flexural modes of the three beams in each pass band. The added foam damping is represented by the dashpot. The approximate mode shapes corresponding to the three modes in each pass band are [1 1 1], [1 0–1] and [1–2 1] in order of increasing frequency. Provided that the pass bands are wide apart, the contribution to the overall response within each pass band from modes in the neighbouring pass bands can be ignored, i.e. modal truncation errors are negligible. Since modes are sampled on all three beams, spatial truncation effects are also negligible. Thus this structure can be idealised as a discrete 3 dof system shown in Fig. 1(b).

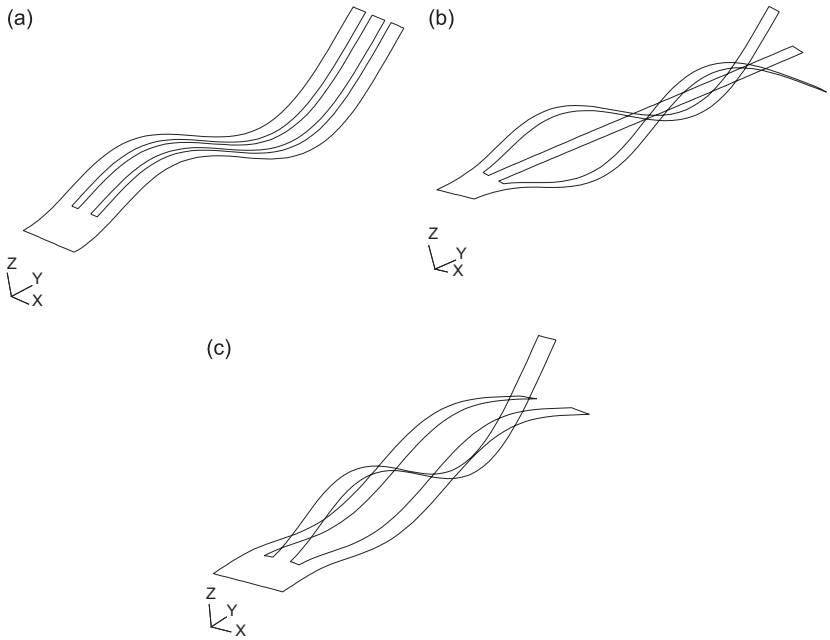

Fig. 2. Mode shapes corresponding to the three modes in the third pass band: (a) Mode 1, (1 1 1); (b) Mode 2, (1 0–1); (c) Mode 3, (1–2 1). It can be noticed that each of the cantilever beams deforms in its third mode in this band. Also notice that the second beam does not deform at all in (b) above, i.e. it is a node.

Table 1
Material and geometric properties of the free–free beam

Beam properties	Numerical values
Length (L)	1.00 m
Width (b)	39.0 mm
Thickness (t)	5.93 mm
Mass density (ρ)	7800 kg/m^3
Young's modulus (E)	2.10 GPa
Cross-sectional area ($a = bt$)	2.3×10^{-4} m^2
Moment of inertia ($I = 1/12bt^3$)	6.8×10^{-10} m^4
Mass per unit length (m)	1.80 kg/m
Bending rigidity (EI)	135.5 N m^2

The second structure is a free–free beam, whose physical properties are as given in Table 1, with constrained layer damping treatment of negligible mass compared to that of the beam applied in a spatially localised region as shown in Fig. 3(b). A viscoelastic polymeric damping foam tape of length 150 mm and width 20 mm was used and it was constrained by a thin steel plate of 1 mm thickness. Care was exercised in supporting the beam to minimise damping from supports. In contrast to the first system, the data from tests on this structure is incomplete in the sense that errors due to truncation and spatial sampling of modes cannot be ignored. The modal overlap factor observed was low, in the range of 0.1–0.2%.

The above two test structures give behaviour representative of a wide range of results which might be obtained in practical modal testing in terms of modal overlap and truncation errors.

3. Test procedure and sources of errors

A description of the hardware used and the data flow in the experiments is shown in Fig. 3(a and b), corresponding to the three cantilever system and the free–free beam, respectively. The source of excitation was

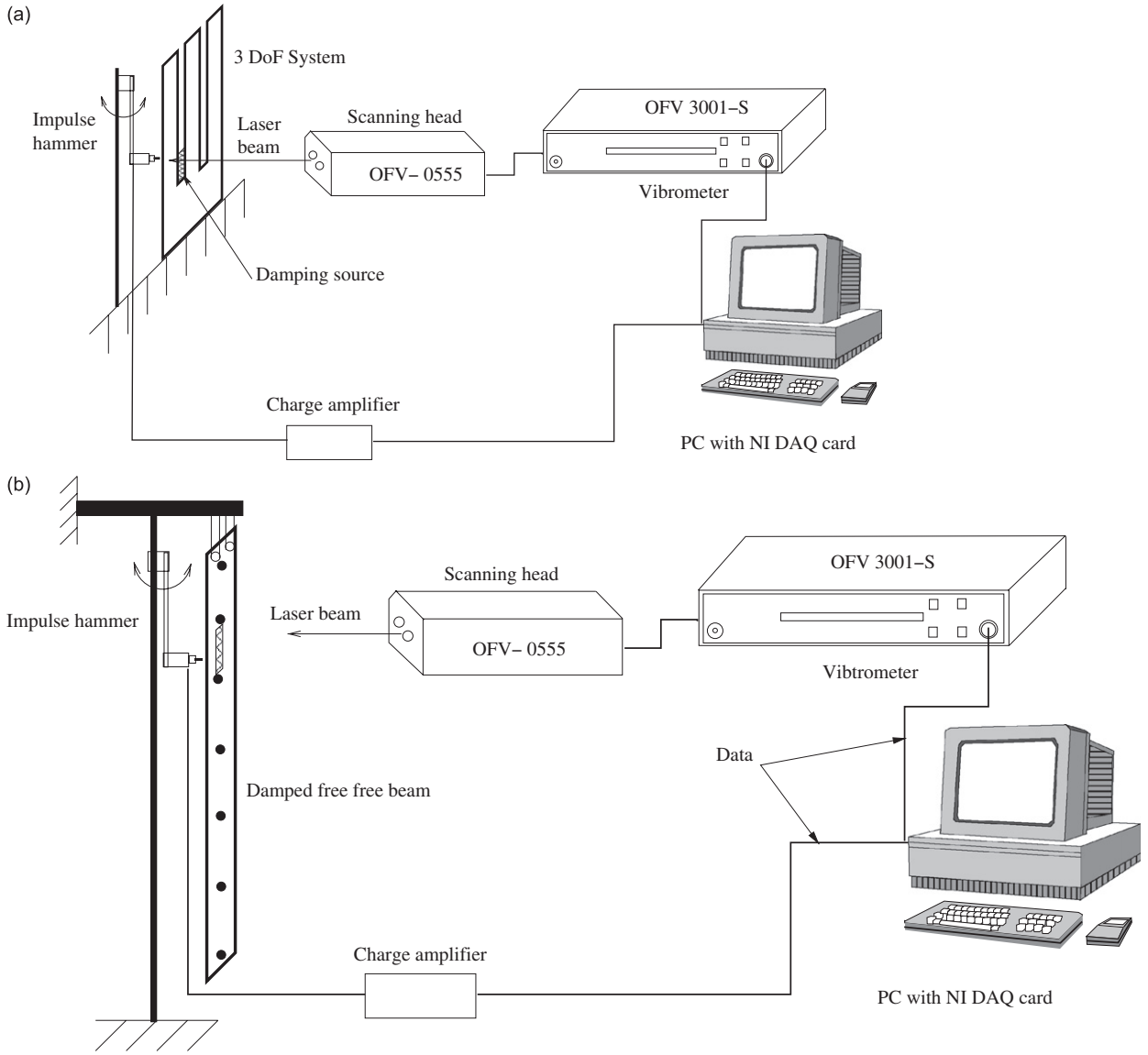

Fig. 3. Experimental set-up: (a) three cantilever structure and (b) free–free beam with the grid points marked as filled dark circles.

an impulse hammer. The hammer was suspended as a pendulum in order to deliver consistent impulses at the same point. The response was measured using a Polytec laser Doppler vibrometer.

The data from the impulse hammer was fed through a charge amplifier and the data from the vibrometer was conditioned using the internal settings of the vibrometer. Both the signals were fed through a NI-DAQ card to the PC (see Ref. [2] for more details). The following procedure was adopted in experiments:

(1) Select a set of force input and response measurement locations. For the three cantilever system three points on the three beams, close to the root of each beam, were chosen. In the case of the free–free beam a set of seven equally spaced grid points were chosen covering the entire length of the beam. The first five flexural modes of the beam, in the frequency range 0–500 Hz, were used in the damping identification. Note that the free–free beam also has rigid body modes at a very low frequency which are not considered here.
(2) Measure the time histories of the force and response for sufficient duration such that the data windowing errors are kept to a minimum.

(3) Calculate the FRFs for each input/measurement combination and average four spectra for each input–output to obtain FRFs showing good coherence over the desired frequency range (0–300 Hz in the case of three cantilever structure and 0–500 Hz in the case of the beam).

It is useful to consider the sources of errors that can have significant impact on the performance of damping identification methods. For a general discussion of sources of errors in modal testing and measures to minimise them see Refs. [3,4]. Here specific errors relevant to damping identification are considered.

Noise in the measurement, due to circuitry and environmental conditions, is one major source of error. In the present experiments, data was measured for sufficiently long duration to capture the entire decaying envelope of the response. This has an undesirable effect on the signal from the impulse hammer. A typical time series for the impulse and the response is shown in Fig. 4. It can be noticed that the voltage signal from the impulse hammer shows a peak at the time of impact and rapidly falls afterwards to a very small value (zero ideally). Once the peak level corresponding to the impulse is passed, the A/D conversion and measurement noise dominate the signal, and this noise appears in the input spectrum leading to noise in the FRF. A cosine taper window [5] was applied to the impulse hammer signal, just outside the region of strong signal, to minimise the A/D conversion noise. Further sources of random noise were minimised by averaging the FRFs for each measurement. The averaged FRF and the associated coherence are shown in Fig. 5.

An important, but often ignored, source of error is the phase error introduced by the instrumentation. Error in phase of the measured transfer function can lead to errors in the complex modes which will influence modal damping identification methods. Conventional ratio calibration tests [3,4] ignore the phase information and seek to determine a real valued ratio calibration factor. However a constant, frequency independent, time delay τ caused by instrumentation, particularly the laser vibrometer and the sequential sampling of channels in the present context, will introduce a linear trend in the phase curve at high frequencies, of the form $\omega\tau$, where ω is the frequency. Thus by fitting a straight line to the phase curve obtained in the calibration tests one can compensate for phase errors of this simple kind. Time delays observed were of the order of 64 μs. In the

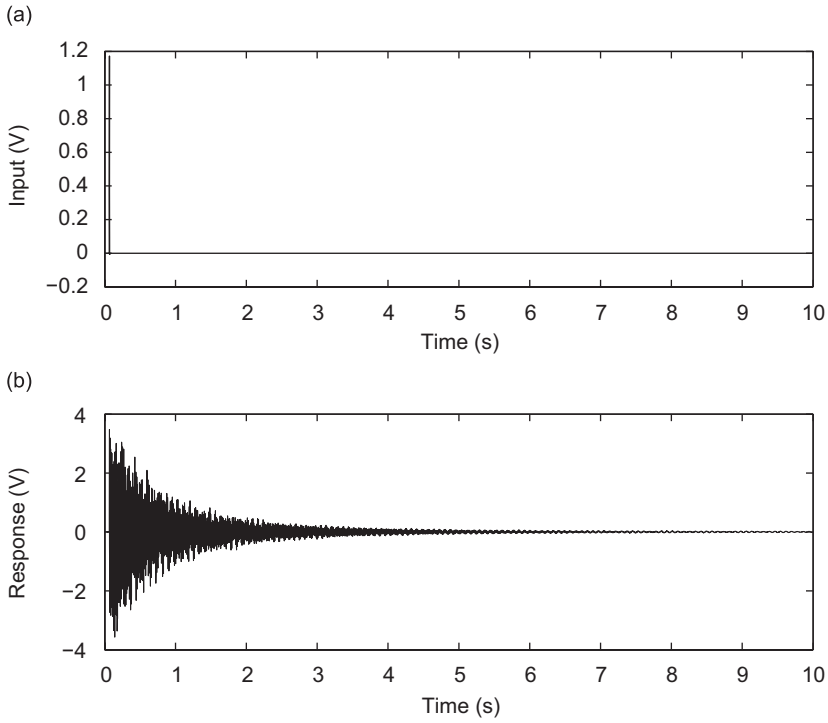

Fig. 4. Typical time series of the experimental data: (a) input impulse and (b) acceleration response. Note that the length of the time window is sufficient enough for all modes in the second and third pass bands to decay. The modes in the first pass band have much lighter damping and hence will need much longer logging time. For this reason, the first pass band will not be considered for further analysis.

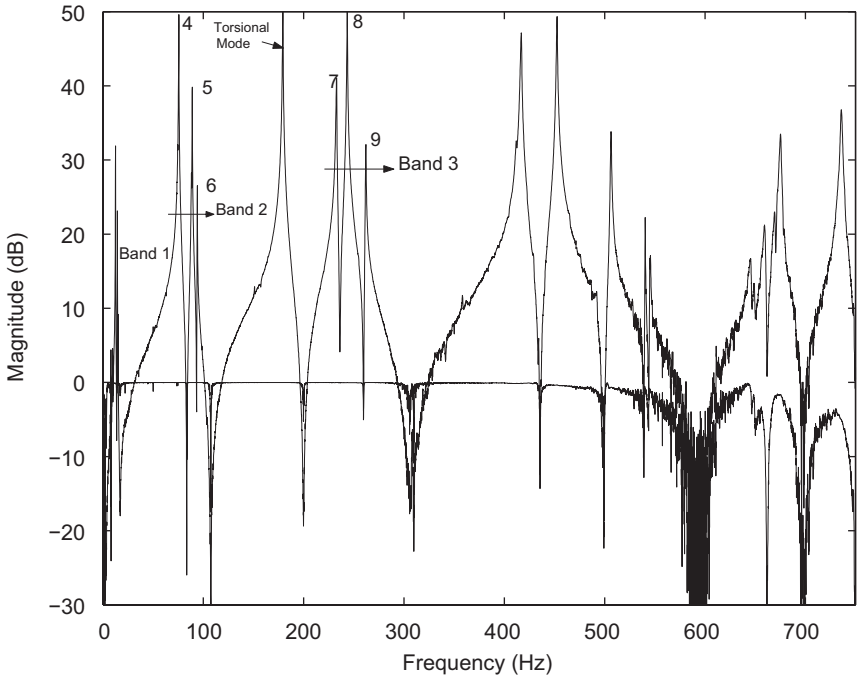

Fig. 5. Typical drive point FRF and the associated coherence measured on the three cantilever system: for calibrated response the magnitude plot must be shifted down by 52 dB.

present work such phase errors were compensated. More details on the calibration apparatus can be found in Ref. [2].

Modal parameter estimation errors were kept to a minimum using a two-stage process. In the first stage each FRF was fitted individually using identification methods such as the circle fitting method and the Rational Fraction Polynomial method. These modal parameters were used as an initial guess to estimate global modal parameters across all the FRFs by solving the full nonlinear least squares problem. Details about the implementation of these methods can be found in Refs. [2–4,6].

All the damping identification methods under investigation assume that the vibrating system is linear. Routine checks on the FRF data such as reciprocity and coherence are employed to assess the linearity of a vibrating structure [3,4]. These checks were ensured in the present experiments: details can be found in Ref. [2]. Finally, it is worth mentioning that the FRF data matrix was symmetrised at every frequency point. This is necessary as small asymmetry of the measured FRF matrix is inevitable in measurements. This will ensure that any asymmetry in the identified damping matrix is due to the identification method alone. With repeatable and clean data on a linear vibrating structure available, one can now apply the damping identification methods using the procedures already described in Ref. [1].

4. Three cantilever structure

Among the damping identification methods of interest to the present study, some methods require that the mass and stiffness matrices of the test structure are known *a priori* (see Ref. [1]). One could take three different approaches to the estimation of the mass and stiffness matrices. In the first approach based on experiments, effective masses for each degree of freedom (dof) are calculated using the drive point FRFs and the mass matrix is deduced therefrom. A second approach is to use some of the identification methods that can identify all three matrices (mass, stiffness and damping) simultaneously. Such methods are: Kim's method, Chen's method and the Instrumental Variable (IV) method. In the third approach, a detailed FE model of the test structure is constructed first and then updated with the measurements using a suitable modal updating procedure [3,4]. Only the first two approaches are discussed in detail here (see Ref. [2] for more details).

The direct experimental approach relies on the calculation of effective masses for each dof using the drive point FRFs. Once the fitted residues are obtained for each mode by modal identification methods for a drive point FRF, the mode shapes $\boldsymbol{\phi}_j$ scaled to unit modal mass can be obtained. The effective mass for dof j is given by $1/\phi_{jj}^2$. From the real parts of the fitted modes one can compute the effective mass defined as above, and hence the mass matrix: see Ref. [3] for further details. The stiffness matrix is calculated using the mode-orthogonality condition. The measured resonant frequencies are used to form a diagonal matrix with the squared natural frequencies forming its entries. This matrix is then transformed back to physical coordinates. The mass and stiffness matrices identified by this method, called the modal method for convenience, are:

$$\mathbf{M}_{\text{modal}} = \begin{bmatrix} 0.18 & -0.03 & 0.04 \\ -0.03 & 0.28 & -0.04 \\ 0.04 & -0.04 & 0.23 \end{bmatrix}, \tag{1a}$$

$$\mathbf{K}_{\text{modal}} = 10^5 \begin{bmatrix} 4.25 & -1.19 & 0.96 \\ -1.19 & 7.27 & -1.22 \\ 0.96 & -1.22 & 5.44 \end{bmatrix}. \tag{1b}$$

There are several possible checks on the accuracy of the above mass and stiffness matrices. Symmetry of the identified matrices is the first check. Clearly, the above matrices are symmetric. One may also compare the measured natural frequencies on the test structure with those obtained by solving the eigenvalue problem:

$$\mathbf{K}\boldsymbol{\phi} = \lambda \mathbf{M}\boldsymbol{\phi}, \tag{2}$$

where $\mathbf{M}$ and $\mathbf{K}$ are the identified mass and stiffness matrix, respectively; λ is the eigenvalue (squared natural frequency) corresponding to the eigenvector $\boldsymbol{\phi}$. Given that the mode-orthogonality conditions were used to compute the stiffness matrix, one naturally expects good agreement between the measured and predicted modal parameters. The above mass and stiffness matrices can be treated as a suitable benchmark to compare with the corresponding matrices identified by the three matrix methods: Kim's method, Chen's method and IV method.

The matrices identified by the three methods from the data in the third pass band (210–270 Hz in Fig. 5) are given below (see Ref. [2] for other pass bands):

$$\mathbf{M}_{\text{kim}} = \begin{bmatrix} 1.37 & 0.37 & -0.26 \\ 0.37 & -20.71 & 3.33 \\ -0.26 & 3.33 & 0.62 \end{bmatrix}, \tag{3a}$$

$$\mathbf{M}_{\text{chen}} = \begin{bmatrix} -0.0012 & 0.0021 & 0.0016 \\ 0.0023 & 0.0020 & 0.0006 \\ -0.0033 & 0.0073 & 0.0871 \end{bmatrix}, \tag{3b}$$

$$\mathbf{M}_{\text{iv}} = \begin{bmatrix} 0.15 & -0.15 & -0.012 \\ -0.03 & 0.18 & 0.03 \\ -0.05 & 0.08 & 0.16 \end{bmatrix} \tag{3c}$$

and

$$\mathbf{K}_{\text{kim}} = 10^7 \begin{bmatrix} -0.31 & -0.07 & 0.07 \\ -0.07 & 5.02 & -0.79 \\ 0.07 & -0.79 & -0.08 \end{bmatrix}, \tag{4a}$$

$$\mathbf{K}_{\text{chen}} = 10^5 \begin{bmatrix} -0.03 & 0.05 & 0.03 \\ 0.07 & 0.03 & -0.16 \\ -0.08 & 0.17 & 2.03 \end{bmatrix}, \tag{4b}$$

$$\mathbf{K}_{\text{iv}} = 10^5 \begin{bmatrix} 3.64 & -3.95 & -0.32 \\ -0.95 & 4.70 & 0.54 \\ -1.17 & 1.51 & 3.68 \end{bmatrix}. \tag{4c}$$

Despite the fact that the input FRF matrix was "symmetrised" the identified mass and stiffness matrices above are not symmetric. It can also be noted that some of the diagonal elements are negative in the case of Chen's method, which is non-physical. This is typical of many identification methods as the constraints of symmetry and positive definiteness on the identified matrices are not explicitly included in their formulation. However this issue is not pursued any further here and merits future work.

It can be deduced, from the comparison of the above identified mass and stiffness matrices in Eq. (4) with those in Eq. (1), that both Kim's method and Chen's method are poor. Only the IV method is close. The same conclusion has been verified by calculating the natural frequencies obtained by solving the eigenvalue problem in Eq. (2). Thus, the modal approach and the IV method are the two best methods of identifying the mass and stiffness matrices from measured FRFs for the present test case.

With the knowledge of the mass and stiffness matrices one can now apply the damping identification methods and compute the measures of performance as defined in Ref. [1]. The four measures of performance are recalled below, for completeness:

(1) To quantify the numerical accuracy of the identified damping matrix the *absolute norm* can be used:

$$N_{\text{abs}} \equiv \left| \frac{\|\mathbf{C}_f - \mathbf{C}\|}{\|\mathbf{C}\|} \right|, \tag{5}$$

where $\mathbf{C}_f$ and $\mathbf{C}$ are, respectively, the fitted damping matrix, and the actual damping matrix, $\|(\bullet)\|$ is the Euclidean or 2-norm of $(\bullet)$, defined for an $N \times N$ matrix $\mathbf{C}$ as $\|\mathbf{C}\| \equiv \sqrt{\sum_{j=1}^{N} \sum_{i=1}^{N} |C_{ij}|^2}$.

(2) The *spatial* norm indicates whether the identified damping matrix has the same qualitative spatial distribution as expected from the distribution of damping sources:

$$N_{\text{spatial}} \equiv \left| \frac{\|\mathbf{C}_f^f - \mathbf{C}^f\|}{\|\mathbf{C}^f\|} \right|, \tag{6}$$

where $\mathbf{C}_f^f$ and $\mathbf{C}^f$ are the spatial *forms* of the fitted and the expected damping matrices in physical coordinates. These matrices are chosen to represent the spatial distribution independent of the magnitudes of damping.

(3) The *modal norm* based on the diagonal part of the identified damping matrix in modal coordinates quantifies the extent to which the damping factors of each mode are fitted:

$$N_{\text{modal}} \equiv \left| \frac{\|\text{diag}(\mathbf{C}'_f) - \text{diag}(\mathbf{C}')\|}{\|\text{diag}(\mathbf{C}')\|} \right|, \tag{7}$$

where $\text{diag}(\mathbf{C}'_f)$, $\text{diag}(\mathbf{C}')$ are matrices containing the diagonal elements of the identified and exact damping matrices in modal coordinates.

(4) The *reconstruction* norm quantifies the fit between the measured FRFs and those synthesised using the identified damping matrix:

$$N_{\text{recon}} \equiv \left\| \frac{|H_r(\omega)| - |H(\omega)|}{|H(\omega)|} \right\|, \tag{8}$$

where H and H_r are the original and the reconstructed FRFs, respectively.

In order to compute the above norms one requires: the actual damping matrix for the absolute norm; modal damping factors and natural frequencies for the modal norm; spatial pattern of the damping matrix for the spatial norm; and the FRFs for the reconstruction norm. Since the actual damping matrix is unknown in experiments (unlike in the simulations where the damping matrix is known *a priori*), the absolute norm cannot be computed. The modal damping factors and the natural frequencies can be identified from the measured data, thus the modal norm can be calculated in experiments. The reconstruction norm can also be computed in experiments. The spatial norm assumes that the spatial distribution of the damping is known *a priori*. In the present experiment, it was observed that the damping was increased by a large factor when the wedged foam was added. So it can be assumed that this foam dominates other damping sources such as material damping and damping from clamped supports. Thus a suitable spatial form for the "added" damping matrix is

$$\mathbf{C}_a = c\begin{bmatrix} 1 & -1 & 0 \\ -1 & 1 & 0 \\ 0 & 0 & 0 \end{bmatrix}, \tag{9}$$

where c is an unknown factor. Using this form, one can compute the spatial norm.

The three norms computed using the data from the third pass band are as shown in Figs. 6(a–c). The norms are plotted on a linear scale and the best identification method has the largest value.

Consider the spatial norm first, shown in Fig. 6(a). Of Adhikari's two methods, the symmetrised viscous fitting method performs better than the original viscous damping identification method. This is consistent with the simulation study results reported in Ref. [1]. Other modal methods such as Lancaster's, Minas's and Ibrahim's methods perform similarly. Except the matrix perturbation method, all matrix methods have similar performance norms. Over all, the matrix perturbation method stands as the best method. It is also clear that the enhanced methods do sometimes (but not always) improve the performance of the original matrix methods. For example, for the IV method the enhanced method based on FRF reconstruction gives a better spatial norm when compared to the original method.

Next consider the modal norm which quantifies the extent to which the identified damping matrices could reproduce the measured damping factors for each mode, as shown in Fig. 6(b). It is immediately obvious that not all methods perform well. The only really successful methods are: Adhikari's modal methods, Chen's method and the Matrix perturbation method. Also, the improvements due to enhanced methods on some matrix methods (Chen's method in particular) are clearly brought out by this norm.

The reconstruction norm shown in Fig. 6(c) reinforces the results shown by the modal norm. To give an idea about how good, or poor, is the quality of reconstruction the synthesised FRF for one input/output location is compared with the measurements in Fig. 7 for two methods: the matrix perturbation method and Kim's method. As will be expected from Fig. 6(c), the matrix perturbation method satisfactorily reproduces the measured data while Kim's method fails to do so.

It can be concluded from these norms that the symmetric viscous fit and Minas and Inman's methods perform better than other modal methods. The methods of Lancaster and Ibrahim are very poor. Among the matrix methods the matrix perturbation method turns out to be the best method with regard to all the norms while Kim's method performs poorly.

4.1. Spatial distribution

Having considered the overall performance of the damping identification methods, the question of spatial distribution of the identified damping matrices is now addressed in more detail. If the damping matrices of the structure before and after adding damping are, respectively, denoted by $\mathbf{C}_u$ and $\mathbf{C}$, then it follows that:

$$\mathbf{C} = \mathbf{C}_u + \mathbf{C}_a, \tag{10}$$

where $\mathbf{C}_a$ is the damping matrix arising due to the addition of damping as given in Eq. (9).

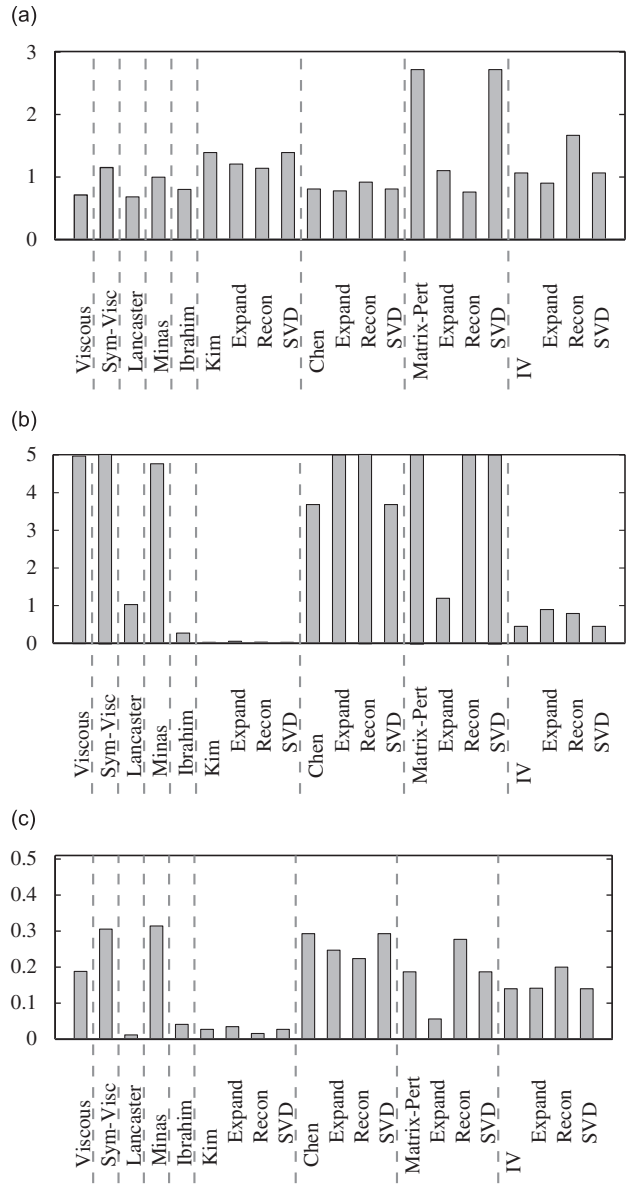

Fig. 6. Norms for the three cantilever system with damping between dofs 1 and 2: (a) spatial norm; (b) modal norm: (c) reconstruction norm. The norm is plotted for various identification methods on a linear scale. The best identification methods are those with large positive values.

In modal coordinates the above equation, for the diagonal terms of the modal damping matrix, implies that

$$\zeta_j \omega_j = \zeta_{uj} \omega_{uj} + \zeta_{aj} \omega_{aj}, \quad j = 1, 2, 3. \tag{11}$$

Here, ω and ζ are the natural frequency and damping factor, respectively. The subscripts *uj* and *aj* refer to the structure without added damping and with the added damping, respectively. In theory, the expected mode shapes of each mode of vibration in the pass band are [1 1 1], [1 0–1] and [1–2 1], respectively. The corresponding measured mode shapes, with added damping, for the third pass band are [1.32 1.21 1.16], [1.85 0.01 –1.63] and [0.75 –1.46 0.72], respectively. These modes are very similar to the ones expected, and for simplicity the theoretical mode shapes will be used in further calculations.

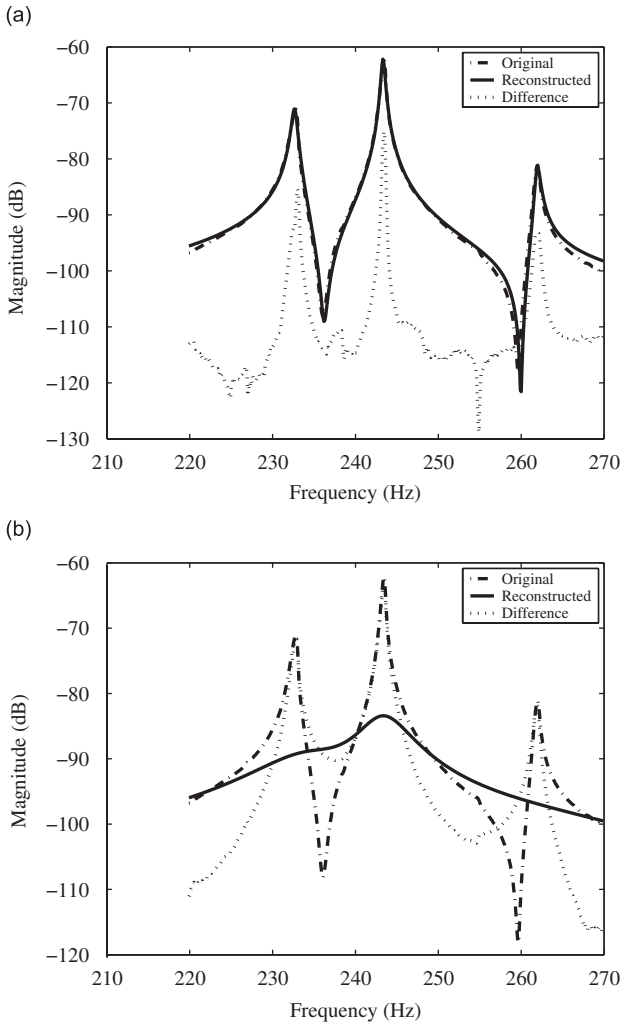

Fig. 7. Comparison of the experimentally measured FRFs and FRFs synthesised using the identified mass, stiffness, and damping matrices for four representative methods: (a) Matrix Perturbation Method and (b) Kim's Method. The data corresponds to the third pass band.

The mass normalised modal matrix, corresponding to the theoretical modes, assuming unit mass matrix, is

$$\mathbf{\Phi}_m = \begin{bmatrix} \frac{1}{\sqrt{3}} & \frac{1}{\sqrt{2}} & \frac{1}{\sqrt{6}} \\ \frac{1}{\sqrt{3}} & 0 & \frac{-2}{\sqrt{6}} \\ \frac{1}{\sqrt{3}} & \frac{-1}{\sqrt{2}} & \frac{1}{\sqrt{6}} \end{bmatrix}. \tag{12}$$

Transforming $\mathbf{C}_a$ in Eq. (9) into modal coordinates one obtains

$$\mathbf{\Phi}_m^{\mathrm{T}} \mathbf{C}_a \mathbf{\Phi}_m = c \begin{bmatrix} 0 & 0 & 0 \\ 0 & \frac{1}{2} & \frac{3}{\sqrt{12}} \\ 0 & \frac{3}{\sqrt{12}} & \frac{3}{2} \end{bmatrix}. \tag{13}$$

The first-order perturbation theory for complex modes [7] states that the diagonal elements of the modal damping matrix are approximately given by $C'_{jj} \approx 2\zeta_j \omega_j$, $j = 1, 2, 3$. Using this relation given by the perturbation theory and the measured modal parameters, one can estimate the unknown parameter c in the

expression for damping matrix in Eq. (9). An estimate for c using the measured data for the third mode is $c = 6(\zeta_{d3}\omega_{d3} - \zeta_{u3}\omega_{u3})/9$, or using the second mode: $c = 2(\zeta_{d2}\omega_{d2} - \zeta_{u2}\omega_{u2})$. Both of them should give the same answer. Here, the subscripts u and d, respectively, denote the undamped and the damped system while the number 2 and 3 refer to the respective modes. A value of 0.8 was obtained for c using the data for both modes.

With this value for c, a final check on the spatial distribution in modal coordinates is given by Eq. (13). It is expected from Eq. (13) that the elements of the damping matrix in the first row/column are small (zero ideally). This can be confirmed by computing the identified modal damping matrix for the added damping. The added modal damping matrix, identified by the matrix perturbation method for the third pass band is

$$\mathbf{C}'_{\text{matper}} = \begin{bmatrix} 0.1262 & 0.0443 & -0.0446 \\ 0.0443 & 0.4119 & 1.2112 \\ -0.0446 & 1.2112 & 1.0574 \end{bmatrix}. \tag{14}$$

It can be noticed that the above matrix broadly agrees with Eq. (13) with regard to the presence of a 2×2 sub-matrix of significantly large numbers in the bottom right corner of the modal damping matrix. This reasonable agreement suggests that the matrix perturbation method is indeed a successful identification method for this experimental case.

5. Free–free beam

This section is concerned with the experiments conducted on a free–free beam. This system differs from the cantilever system in two important aspects:

(1) The modal overlap is much lower (typically 0.1–0.2%) compared to the three cantilever system, which means that the modes are expected to be less complex.
(2) Continuous vibration mode shapes are sampled at a set of measurement points and hence errors due to the spatial sampling of modes are present in this data. Since only the first few modes are considered for damping identification, modal truncation errors are also present.

A sketch of the experimental set-up is shown in Fig. 3(b). A constrained layer damping treatment of negligible mass compared to the total mass of the beam was applied as shown in Fig. 3(b). For the purpose of FRF measurements, seven equally spaced grid points on the beam were chosen, which are shown in Fig. 3(b) as dark circles. Data checks such as coherence and reciprocity were carried out to ensure that data was of good quality as discussed in the context of the three cantilever structure: see Ref. [2] for details. The full 7×7 FRF matrix was measured using impulse hammer and Polytec laser vibrometer.

After having obtained good quality measurements, the mass and stiffness matrices need to be identified. In contrast with the cantilever systems, which can be modelled as a discrete system in each pass band, the free–free beam is a continuous system. Spatial truncation is important, and one requires mass and stiffness matrices of size 7×7 corresponding to the 7 measurement points. These matrices can be identified using the methods described in the earlier Section 4. In addition to these, a finite element model was also constructed using beam elements, given the simplicity of the test structure. The mass and stiffness matrices of this model were reduced to the required size, using the iterated IRS technique [8]. As in the case of the three cantilever system, one can also obtain the mass and stiffness matrices using the identification techniques: Kim, Chen and the IV method.

In order to test the accuracy of the identified matrices the eigenvalue problem in Eq. (2) is solved, and the resulting frequencies are compared with measured values in Table 2. It can be seen that among the identification methods, only the IV method gives mass and stiffness matrices in reasonable agreement with the measured natural frequencies. Nevertheless, the mass and stiffness matrices obtained from the FE model were found to be more accurate. Hence, these were used as an input to those damping identification methods which require *a priori* knowledge of the mass and stiffness matrices (see Ref. [1]).

Table 2
Comparison of natural frequencies calculated from the eigenvalue problem determined by the identified mass and stiffness matrices

Mode	Beam theory	Measured	Kim's method	Chen's method	IV method	FE model
1	30.6	33.01	$6.56 - 115.51i$	53.52	34.51	30.87
2	85.1	85.04	$55.59 + 1.16i$	118.61	82.71	85.22
3	166.8	166.0	$165.78i$	225.64	166.76	167.75
4	275.8	275.81	$35.06 + 186.56i$	398.51	285.99	279.2

The "measured" values are obtained by modal fitting. Note that the reduced FE model is the best of all. All numerical values are in Hz.

The three measures of performance—spatial, modal and reconstruction norms—were computed based on the identification results of each method and they are plotted in Fig. 8(a–c). The spatial norm, shown in Fig. 8(a), is based on the assumption that damping in the beam is mostly from the constrained layer patch between measurement locations 2 and 3. Thus the reference matrix for this norm is a damping matrix which contains a 2×2 sub-matrix of non-zero elements corresponding to the locations 2 and 3, and all other elements set to zero. The methods that perform better with respect to this norm are Lancaster's method among modal methods and Matrix perturbation method among the matrix methods. Adhikari's methods, which rely on accurate identification of complex modes, do not perform well.

With regard to the modal norm, shown in Fig. 8(b), the best methods are: Adhikari's viscous and symmetrised viscous methods and the matrix perturbation method. Note that in Adhikari's methods, only the off-diagonal part of the modal damping matrix is identified. The diagonal part is directly deduced from the measured modal parameters. Thus, even though the spatial distribution may not be accurate the individual decay rates of each mode are well-fitted as reflected in the modal norm. Some matrix methods such as Kim's, Chen's and IV method show moderate values of the norms, indicating that the modal damping factors are not too far off from measured values.

The successful methods with regard to the reconstruction norm, shown in Fig. 8(c), are the matrix perturbation method, Kim's method, Chen's method and the IV method. The benefit of the enhanced method based on FRF expansion in the case of Chen's method and the IV method can be observed. None of the modal methods were successful. Although Lancaster's method seems to perform well with regard to the spatial norm, it failed to fit the decay rates of individual modes as reflected in the modal norm and hence also performed poorly with respect to the reconstruction norm.

In summary the matrix perturbation method and the IV method are the two best methods that perform consistently with respect to all the three norms. As expected from the earlier simulation study [1], the pattern of success and failure among the different methods is different from that found with the three-cantilever system.

5.1. Identification of complex modes

It is worth remembering that the success of modal methods, such as Adhikari's methods, is closely tied to the accuracy with which complex modes can be identified in experiments. A brief review of complex modes and their role in identifying damping models in linear vibration theory is useful to judge the applicability of these methods in practical tests.

Complex modes are widely observed in vibration tests. The usual practice in the vibration testing community is to ignore complex modes and convert them to the "best" real modes for comparison with FE models. This section will attempt to address the core issue of identification of complex modes from measured vibration data. Experiments conducted on the free–free beam are used. Two aspects of the complex modes are of interest in this context. The first concerns the "shape" of the complex modes while the second and more important aspect concerns repeatability.

Consider the shape of a complex mode in the case when the undamped modes are scaled to unit modal mass. It is expected from the first-order perturbation theory [7] that, provided damping is viscous and small, the "shape" of the imaginary part of a complex mode is a weighted sum of the real mode shapes of the

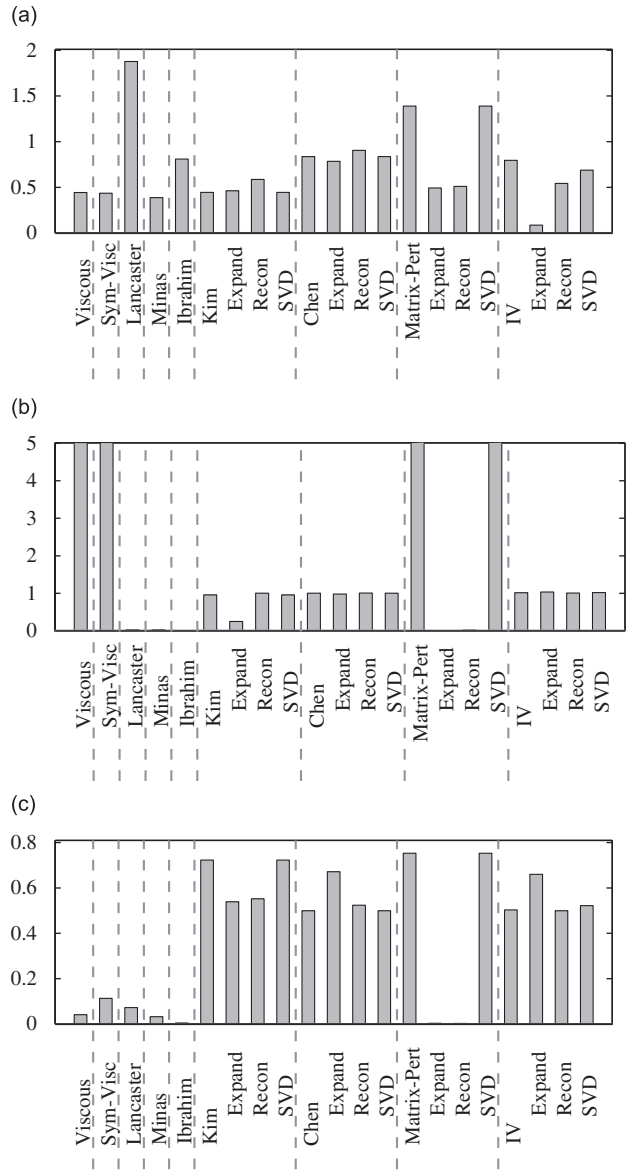

Fig. 8. The three norms for the beam data: (a) spatial norm; (b) modal norm: (c) reconstruction norm. The norm is plotted for various identification methods on a linear scale. The best identification methods are those with large positive values.

neighbouring modes (see Ref. [1]). The modes that are closer in frequency contribute more to the imaginary part of the complex mode than those lying far away. For example, in the case of a free–free beam with well separated modes and light damping one expects that the "shape" of the imaginary part of the first mode ought to resemble that of the real part of the second mode, with progressively smaller contributions from the real mode shapes of the higher modes.

In light of the above qualitative features of complex modes from the perturbation theory, the symmetry behaviour of modeshapes is of interest in the present experiment. Real mode shapes are alternately symmetric and antisymmetric. The imaginary parts of a given mode shape should be dominated by neighbouring modes, on both sides, and these always have opposite symmetry to the real mode. So a symmetric real part is expected to correspond, approximately, to an antisymmetric imaginary part and vice versa.

The second, and possibly more crucial, issue regarding the measurement of complex modes is that of repeatability. Given that the full 7×7 FRF matrix was measured for the free–free beam, one can apply modal

identification methods to each row/column of the FRF matrix separately to identify the complex natural frequencies and residues. The fitted complex residues can be used to identify the complex mode shapes. Ideally, the same answer should be found in each case.

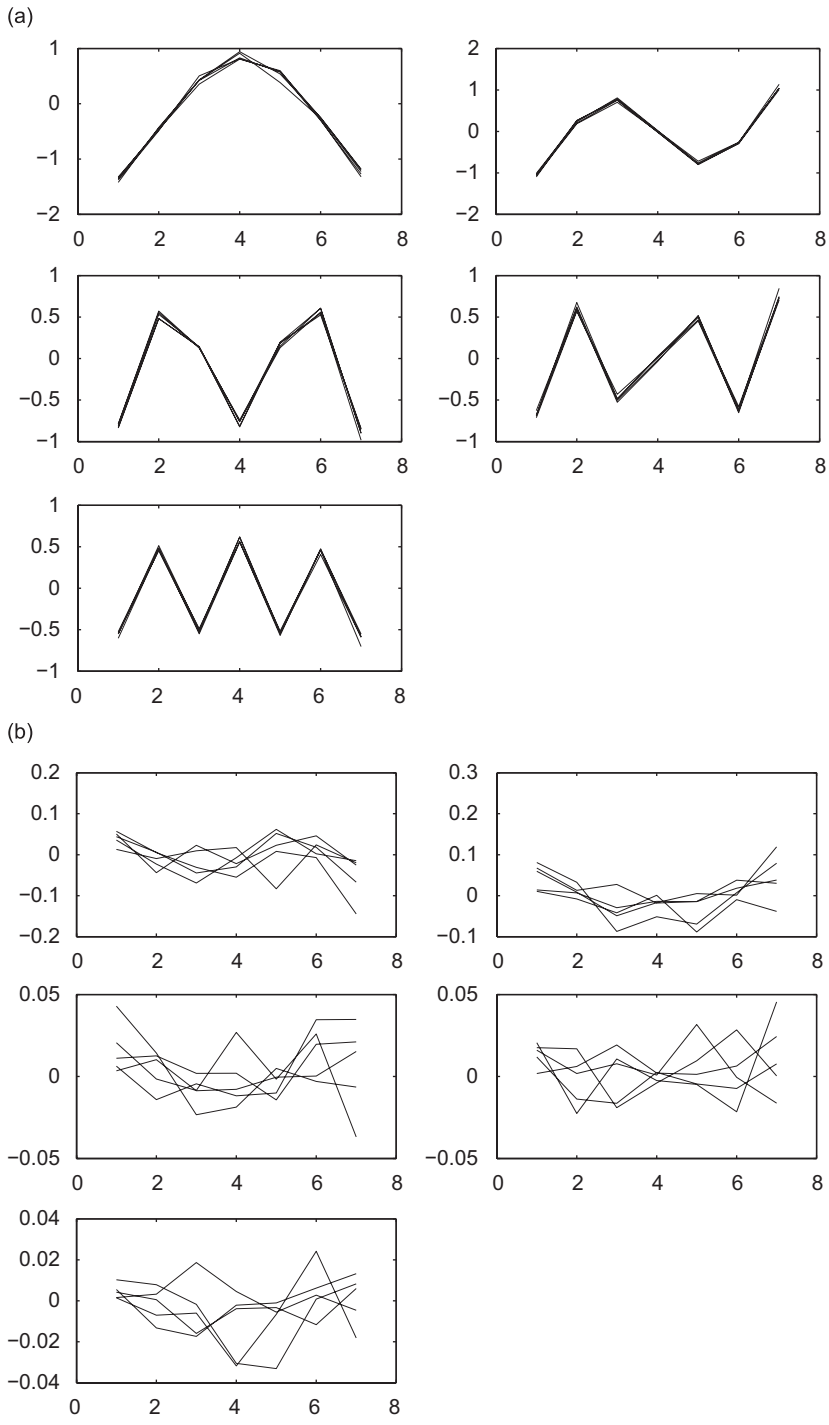

Fig. 9. Identified complex modes of the free–free beam from various rows of the FRF matrix: (a) real part and (b) imaginary part.

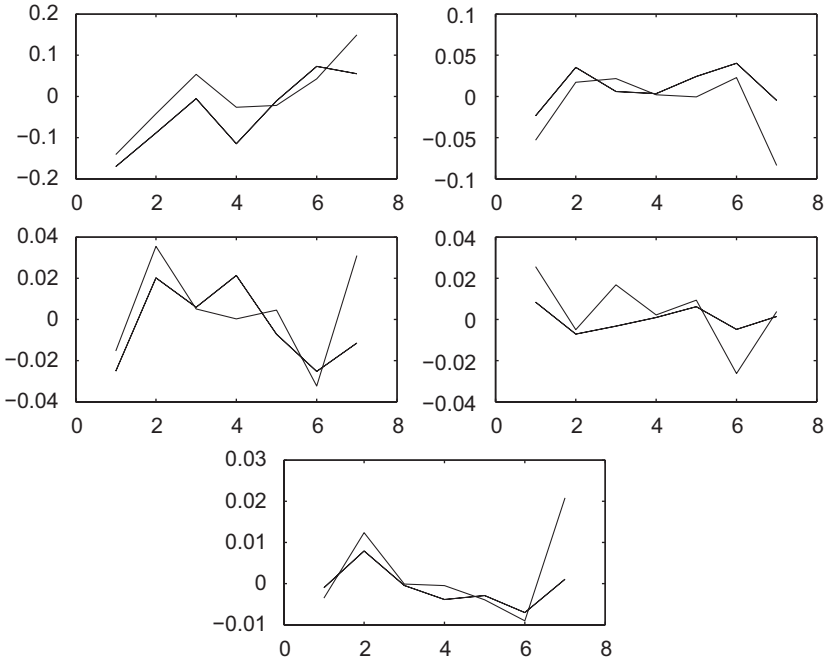

Fig. 10. Comparison of the imaginary part of the complex modes identified from two rows of the FRF matrix measured on the free–free beam with damping treatment applied over half its length.

The identified real and imaginary part of the first five modes, from each of the seven rows of the FRF data, are shown in Fig. 9. While the repeatability of the real part of the modes is very good, the same cannot be said about the imaginary parts. The first two modes show a hint of the expected symmetry behaviour, but it is not very convincing.

To further investigate this qualitative aspect of complex modes, the level of damping in the beam was increased by covering both sides of the beam with damping material over half its length. The added mass due to damping is duly accounted in the analysis. The identified complex modes for this beam from two rows of the FRF matrix are as shown in Fig. 10. It is clear from these results that the complex modes are again difficult to measure reliably. However, qualitative "shapes" of these modes do follow the perturbation theory results. This time, the expected pattern of shapes can be followed higher in the mode sequence.

The correlation among the real and imaginary parts of the complex modes can be quantified by the modal assurance criterion (MAC) [3]. Here, MAC between two sets of complex modes denoted by $\boldsymbol{\psi}$ and $\boldsymbol{\psi}'$ is defined as

$$\mathrm{MAC} = \frac{|\sum_{j=1}^{N} \boldsymbol{\psi}_j' \boldsymbol{\psi}_j^{\mathrm{H}}|^2}{(\sum_{j=1}^{N} \boldsymbol{\psi}_j \boldsymbol{\psi}_j^{\mathrm{H}})(\sum_{j=1}^{N} \boldsymbol{\psi}_j' \boldsymbol{\psi}_j'^{\mathrm{H}})}, \tag{15}$$

where $()^{\mathrm{H}}$ denotes the Hermitian transpose of a complex vector. If the modes are well correlated, the MAC matrix should approximate to a unit diagonal matrix. By choosing the complex modes identified from the first row of the FRF matrix as a reference, the MAC matrix is computed for each row, with results as shown in Fig. 11 for the real and imaginary parts of the complex modes. It is clear from this figure that only the real parts of the modes are well correlated while the imaginary parts are not. Again this confirms the difficulty of reliable identification of complex modes.

Unfortunately the level of variability seen in Fig. 9 is not adequate to identify the sensitive parameters of a damping model. Thus, the identification methods based on complex modes are bound to suffer in experiments. It seems debatable whether damping identification methods based on complex modes will ever work in practice.

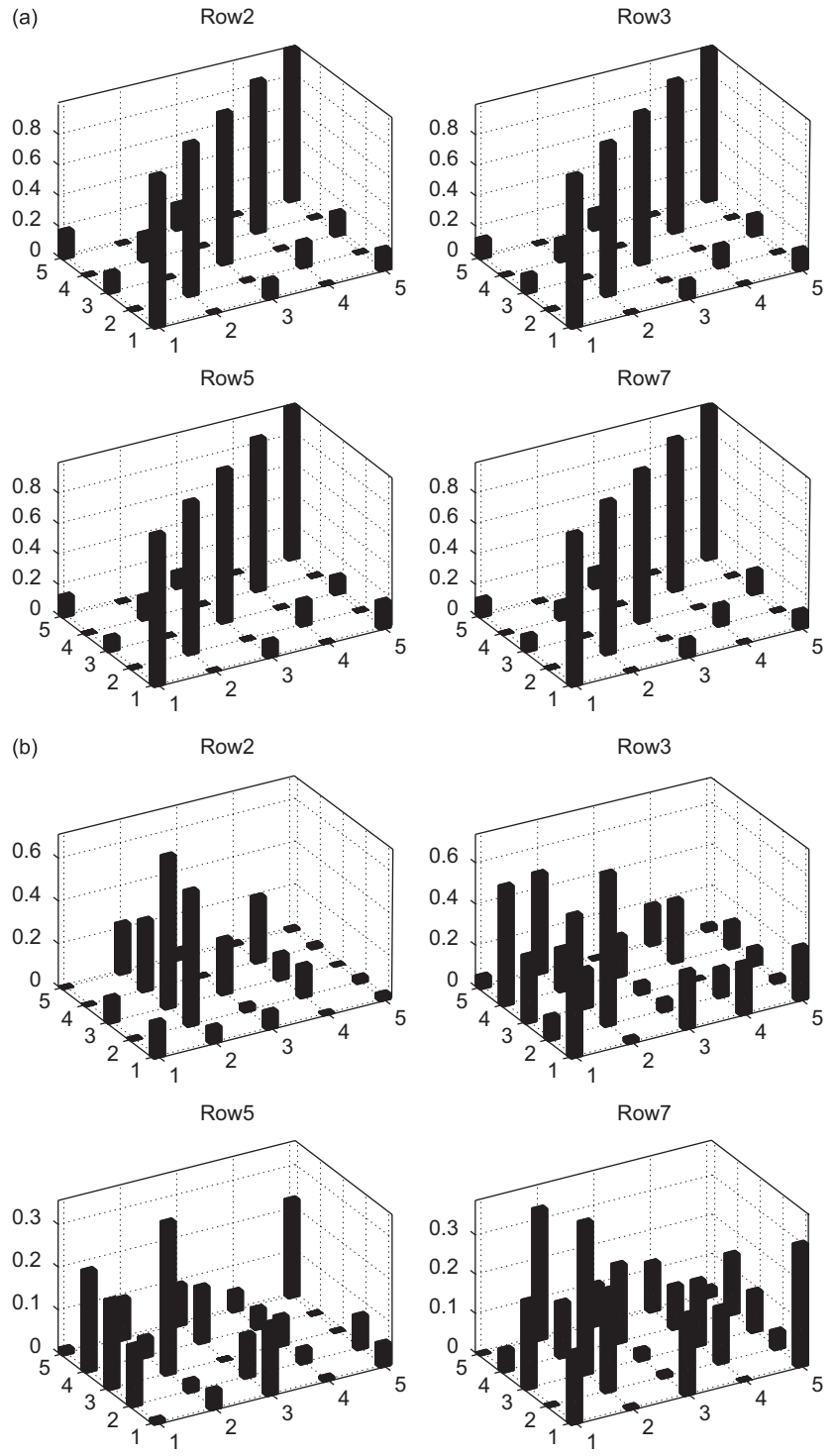

Fig. 11. MAC for complex modes identified from various rows of FRFs corresponding to various points of excitation along the length of the beam: (a) real part and (b) imaginary part. The first row data is used as a reference.

6. Conclusions

In this work the performance of a range of viscous damping identification methods on two experimental systems of different modal overlap factors has been studied. The following conclusions emerge.

(1) When the errors due to modal truncation and spatial sampling of modes are negligible, as in the case of the experiments on the three cantilever system, the identification methods that perform well with respect to the reconstruction norm are: Adhikari's symmetrised viscous fit, Minas and Inman's method, Chen's method, the matrix perturbation method and the IV method. However, of all the above methods, only the matrix perturbation method was found to satisfactorily reproduce the spatial distribution of damping. Enhanced methods were found to be useful only with the IV method.
(2) Accurate fitting of FRFs does not automatically ensure that the spatial distribution of damping is well fitted. This is consistent with the conclusions from the simulation study reported in Ref. [1].
(3) When the errors due to modal truncation and spatial sampling of modes are significant, and the structure has low modal overlap, as is the case with experiments on the free–free beam, it is found that modal methods fail to perform well. This is mainly due to errors in measurements of complex modes. Among the matrix methods which seek to identify the mass, stiffness and damping matrices simultaneously, only the IV method was successful in experiments. Enhanced methods in general do not produce any clear gains.
(4) Complex modes for a system with low modal overlap are difficult to measure and not repeatable as shown by free–free beam tests. Hence damping identification methods based on complex modes must be viewed with skepticism.

References

[1] A.S. Phani, J. Woodhouse, Viscous damping identification in linear vibration, *Journal of Sound and Vibration* 303 (3–5) (2007) 475–500.
[2] A.S. Phani, Damping Identification in Linear Vibrations, PhD Thesis, Cambridge University Engineering Department, Trumpington Street, Cambridge, CB2 1PZ, January 2004.
[3] D.J. Ewins, *Modal Testing*, second ed., Research Studies Press Ltd., Taunton, Somerset, England, 2000.
[4] N.M. Maia, J. Silva (Eds.), *Theoretical and Experimental Modal Analysis*, first ed., Research Studies Press Ltd., Taunton, Somerset, England, 2000.
[5] K.G. McConnell, *Vibration Testing: Theory and Practice*, first ed., Wiley Interscience, New York, 1995.
[6] P. Duffour, Noise Generation in Vehicle Brakes, PhD Thesis, Cambridge University Engineering Department, Trumpington Street, Cambridge, CB2 1PZ, December 2002.
[7] J. Woodhouse, Linear damping models for structural vibration, *Journal of Sound and Vibration* 215 (3) (1998) 547–569.
[8] M.I. Friswell, S.D. Garvey, J.E.T. Penny, Model reduction using dynamic and iterated irs techniques, *Journal of Sound and Vibration* 186 (2) (1995) 311–323.